Structural and vibrational properties of $Ba_xSr_{1-x}TiO_3$ nanoparticles

C. T. LEE, M. S. ZHANG*, Z. YIN, W. ZHU
National Laboratory of Solid State Microstructures, and Centre for Materials Analysis, Nanjing University, Nanjing 210093, People's Republic of China
E-mail: mszhang@nju.edu.cn

$Ba_xSr_{1-x}TiO_3$ (BST) is an important mixed alloy material, showing extensive applications in DRAM capacitors, phase shifters, phase array antennas, thermistors and pyroelectric detectors [1–4]. Much of the research work has concerned structural properties in the bulk and films [5–7]. Driven by applications of nanostructures in ferroelectric fields, research on $Ba_xSr_{1-x}TiO_3$ ultra-fine particles is a promising subject. Many techniques, such as sol-gel, hydrothermal synthesis, stearic acid, solid state reaction, etc. have been used to prepare nanoparticles. Among them the stearic acid method offers a unique advantage: extra-fine nanocrystals can be easily prepared with a stoichiometric constitution due to the lower decomposition temperature [10–12]. It was reported that uniformly sphere-like $Ba_xSr_{1-x}TiO_3$ nanoparticles (about 50 nm) were synthesized by the stearic acid method and the transition temperature decreased with decreasing grain size [8, 9]. In this paper, we use the stearic acid technique to prepare $Ba_xSr_{1-x}TiO_3$ nanoparticles. We study the phase structure and the relative tetragonality c/a by X-ray diffraction, and the vibrational properties via both Raman and IR spectroscopy. We pay special attention to the doping effect of different Ba concentrations.

$Ba_xSr_{1-x}TiO_3$ nanoparticles were synthesized at room temperature by the stearic acid method with barium stearate, strontium stearate and $(C_4H_9O)_4Ti$ as the precursor materials. The process involved dissolving the barium stearate and strontium stearate in the stearate solvent, adding $(C_4H_9O)_4Ti$ into the solution and fully mixing, and finally annealing at 750 °C for 1 h to form $Ba_xSr_{1-x}TiO_3$ nanoparticles.

The phase structures were examined on a Rigaku X-ray diffractometer with Cu K_α as the incident radiation. Raman spectral measurement was conducted on a J.Y HR-800 Raman spectrometer, and 488 nm excitation was used from an air-cooled argon laser with 16 mW output, and IR spectral measurements were performed on a Nicolet Nexus 870 Fourier Transform Infrared (FT-IR) Spectrometer.

The XRD patterns of $Ba_xSr_{1-x}TiO_3$ nanoparticles from $x = 0.0$ to 0.3 one plotted in Fig. 1. All the four nanoparticles show sharp peaks of (100), (110), (111), (200), (210) and (211), which indicates good crystallinity in the cubic phase. The average grain sizes were 34, 32, 25 and 23 nm for $x = 0.0$, 0.1, 0.2 and 0.3, respectively which were obtained via Scherrer's formula [13] $D = k\lambda/(\beta \cos\theta)$, where k is the constant (shape factor about 1.0), λ the X-ray wavelength (1.542 Å), β the FWHM of the (110) diffraction line and θ the diffraction angle. It can be seen that the average grain size decreases with increasing Ba doping. It is known that crystal growth is involved in the motion of the grain boundaries which can be "pinned" by introducing tiny secondary-phase particles [14]. In preparation of $Ba_xSr_{1-x}TiO_3$ nanoparticles by the stearic acid method, there is excess barium (i.e. Ba/Ti > 1) on the surface of the nanoparticles. With increasing Ba concentration more and more barium atoms inhibit the growth of the grains [15, 16], leading to reduction in the growth rate and gradual saturation. This situation is similar to the case of La-doped $PbTiO_3$ nanoparticles [17].

Raman spectra of $Ba_xSr_{1-x}TiO_3$ nanoparticles at various Ba concentrations are shown in Fig. 2. where a broad-band structure was recorded, which corresponds to a background for the "one–phonon" bands due to the existence of a relaxation process [18]. The Raman spectrum in $SrTiO_3$ bulk is entirely second-order in the cubic perovskite [19]. The appearance of first-order Raman lines of 171, 537 and 790 cm^{-1} in $Ba_xSr_{1-x}TiO_3$ nanoparticles, indicates a lower crystal symmetry induced by impurities and defects and the Raman selection rule was relaxed in comparison with $SrTiO_3$ bulk [19, 20]. As x increases to 0.3, all the modes at 243, 283, 537, 615 and 790 cm^{-1} downshift to 231, 279, 525, 591 and 760 cm^{-1}, respectively. In single crystal $SrTiO_3$, the second-order Raman lines at 243, 283 and 615 cm^{-1} shift downward when the temperature approaches T_c [19]. We attributed the mode softening in $Ba_xSr_{1-x}TiO_3$ nanoparticles to enhancement of the tetragonality c/a with increasing Ba concentration.

Fig. 3 depicts the variation of lattice constants a and c, and the tetragonality c/a for $Ba_xSr_{1-x}TiO_3$ nanoparticles, as a function of Ba concentration. With increasing Ba concentration, lattice constant a increases a little, but c increases greatly, leading to an appreciable increase in tetragonality. The c/a value gradually increases from 1.001 to 1.007 at $x = 0.3$, which implies $Ba_xSr_{1-x}TiO_3$ nanoparticles deviate from the original pseudo-ferroelectric structure for $SrTiO_3$, the tetragonality being smaller than that of weak ferroelectrics $BaTiO_3$ ($c/a = 1.01$) [21]. It is known that the cubic phase of $SrTiO_3$ is stabilized by hydrostatic pressure due to shrinking of the unit cell [22, 23]. The substitution of Sr^{2+} by Ba^{2+} enlarges the unit cell [23] and strengthens the tetragonality.

*Author to whom all correspondence should be addressed.

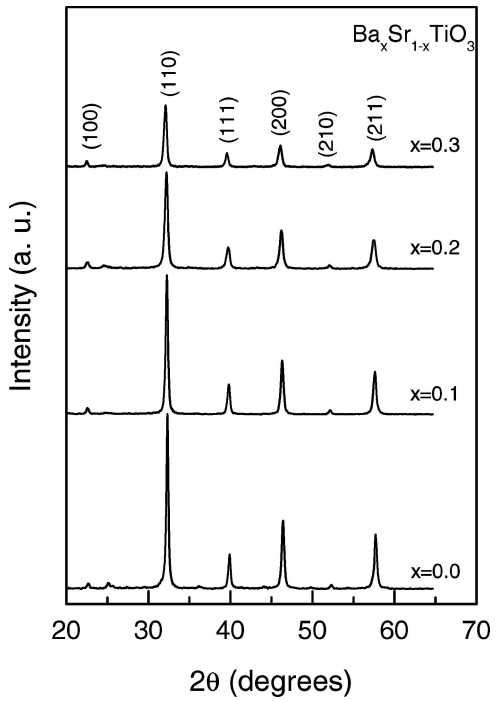

Figure 1 XRD patterns of $Ba_xSr_{1-x}TiO_3$ nanoparticles at various Ba concentrations.

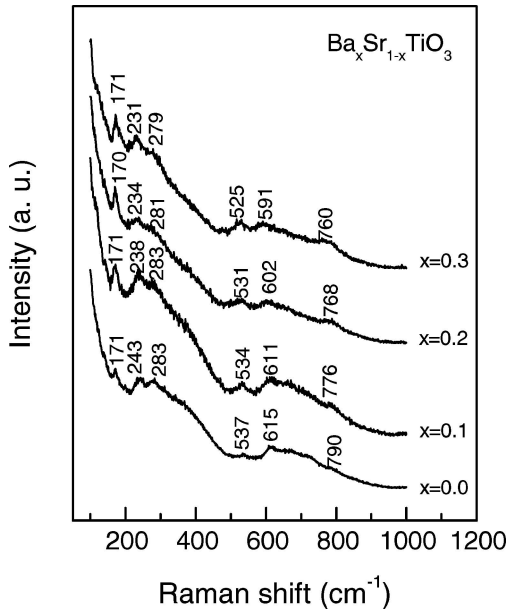

Figure 2 Raman spectra of $Ba_xSr_{1-x}TiO_3$ nanoparticles at various Ba concentrations.

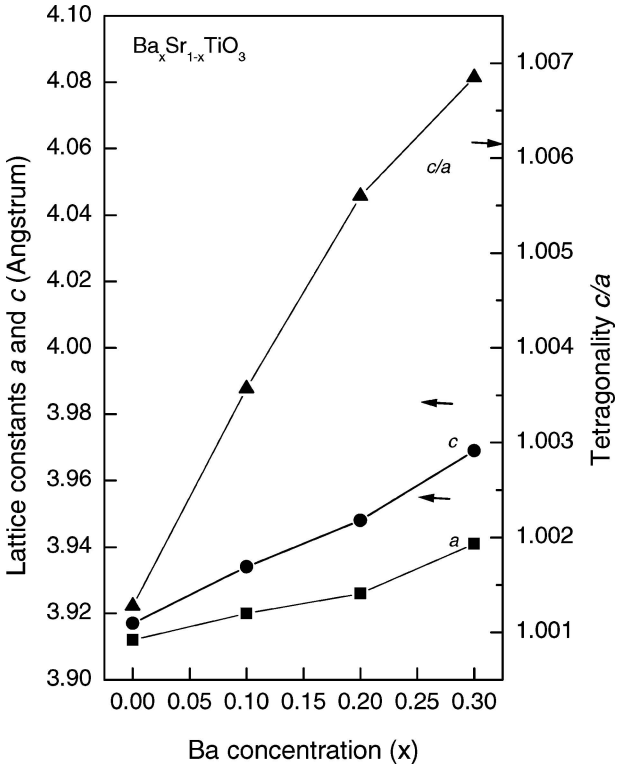

Figure 3 Tetragonality c/a of $Ba_xSr_{1-x}TiO_3$ nanoparticles as a function of Ba concentration.

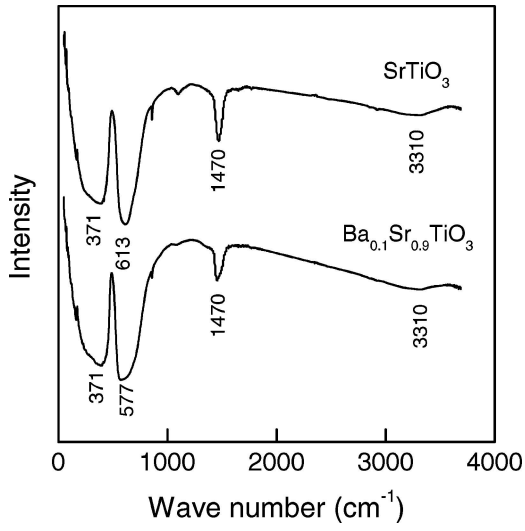

Figure 4 IR spectra of both $SrTiO_3$ and $Ba_{0.1}Sr_{0.9}TiO_3$ nanoparticles.

Fig. 4 shows the IR spectra for both $SrTiO_3$ and $Ba_{0.1}Sr_{0.9}TiO_3$ nanoparticles. There are four absorption bands at 3310, 1470, 613 and 371 cm^{-1} in $SrTiO_3$ specimen, and at 3310, 1470, 577 and 371 cm^{-1} in $Ba_{0.1}Sr_{0.9}TiO_3$ nanoparticles. These two curves show that the stretching mode of internal OH^- at 3310 cm^{-1}, the C═O vibration mode at 1470 cm^{-1} and the O─Ti─O 'bending' mode at 371 cm^{-1} [24] did not show frequency shifts; whereas the 613 Ti─O stretching mode [24] downshifts to 577 cm^{-1}. We attribute the downshift of the 613 cm^{-1} mode to the increase in tetragonality by Ba substitution. The 'bending' vibration band at 371 cm^{-1}, which exists only for the titanate-KBr pellet, is still considered as a scattering effect, but not a real absorption band [25, 26].

In conclusion, we have successfully synthesized $Ba_xSr_{1-x}TiO_3$ nanoparticles by the stearic acid method. Raman spectra show broad-band shapes, which is attributed to the background induced by relaxation process. Comparing with $SrTiO_3$ bulk material, the lower symmetry induced by impurities and defects in $Ba_xSr_{1-x}TiO_3$ nanoparticles leads to the appearance of first-order Raman lines. Ba substitution increases the c/a value from 1.001 to 1.007 at $x = 0.3$, most of the Raman frequencies and the IR 613 cm^{-1} mode shift downward.

Acknowledgements

The work was supported by the National Natural Science Foundation of China, through Grants No. 10174034 and No. 10374047, and the Natural Science Foundation of Jiangsu Province.

References

1. C. HANSAN and H. BERATAN, Proceedings of the Ninth IEEE International Symposium on Applied Ferroelectrics (IEEE, New York, 1995) p. 657.
2. L. C. SENGUPTA, E. NGO, J. SYNOWEZYNSKI and S. SENGUPTA, Proceedings of the Tenth IEEE International Symposium on Applied Ferroelectrics (IEEE, New York, 1996) p. 845.
3. Z. G. BAN and S. P. ALPAY, *J. Appl. Phys.* **93** (2003) 504.
4. E. H. LEE, J. SOK, *et al.*, *Supercond. Sci. Technol.* **12** (1999) 981.
5. L. BENGUIGUI and K. BETHE, *J. Appl. Phys.* **47** (1976) 2787.
6. P. PASIERB, S. KOMORNICKI and M. RADECKA, *Thin Solid Film* **324** (1998) 134.
7. C. B. SAMANTARAY, A. ROY, M. ROY, M. L. MUKHERJEE and S. K. RAY, *J. Phys. Chem. Solids* **63** (2002) 65.
8. X. H. WANG, The Structures and Properties of Perovskite-Type Titanate Composite Oxides of Nanocrystalline Materials, PhD Dissertation, Shandong University, China, 1994, p. 65.
9. L. ZHANG, W. L ZHONG, C. L. WANG and Y. G. WANG, *J. Phys.* D **32** (1999) 546.
10. J. F. MENG, J. P. LI, G. T. ZOU, X. H. WANG, Z. C. WANG and M. Y. ZHAO, *Chin. Phys. Lett.* **11** (1994) 345.
11. T. L. REN, P. L. ZHANG, W. L. ZHONG, X. H. WANG and B. K. XU, *ibid.* **11** (1994) 310.
12. X. H. WANG, C. ZHAO, Z. WANG and M. Y. ZHAO, *J. Alloys Comp.* **204** (1994) 33.
13. L. S. BIRKS and H. FRIEDMAN, *J. Appl. Phys.* **17** (1946) 687.
14. N. L. WU, S. Y. WANG and I. A. RUSAKOVA, *Science* **285** (1999) 1375.
15. T. L. REN, J. L. ZHU, J. J. XIONG, X. H. WANG and L. T. LI, *J. Funct. Math.* **29** (1998) 69.
16. X. H. WANG, The Structures and Properties of Perovskite-Type Titanate Composite Oxides of Nanocrystalline Materials, PhD Dissertation, Shandong University, China, 1994, p. 159.
17. Y. DENG, Z. YIN, Q. CHEN, M. S. ZHANG and W. F. ZHANG, *Matt. Sci. Eng.* B **84** (2001) 250.
18. J. I. DOS SANTOS and G. A. BARBOSA, *Ferroelectrics* **25** (1980) 627.
19. W. G. NILSEN and J. G. SKINNE, *J. Chem. Phys.* **48** (1967) 2240.
20. H. UWE *et al.*, *Ferroelectrics* **96** (1989) 123.
21. R. E. COHEN, *Nature* **358** (1992) 137.
22. R. P. LOWNDES and A. RASTOGI, *J. Phys.* C **6** (1973) 932.
23. L. ZHANG, W. L. ZHONG, Y. G. WANG and P. L. ZHANG, *Solid State Commun.* **104** (1997) 264.
24. J. T. LAST, *Phys. Rev.* **105** (1957) 1743.
25. W. G. SPITZER, ROBERT C. MILLER, D. A. KLEINMAN and L. E. HOWARTH, *ibid.* **126** (1962) 1719.
26. J. M. BALLANTYNE, *ibid.* A**136** (1964) 433.

Received 3 May
and accepted 23 June 2004